

Supernova Neutrino-Nucleus Physics and the r-process

W. C. Haxton

Institute for Nuclear Theory and Department of Physics

Box 351550, University of Washington

Seattle, WA 98155

E-mail: haxton@phys.washington.edu

June 13, 2018

Abstract

This talk reviews three inputs important to neutrino-induced nucleosynthesis in a supernova: 1) “standard” properties of the supernova neutrino flux, 2) effects of phenomena like neutrino oscillations on that flux, and 3) nuclear structure issues in estimating cross sections for neutrino-nucleus interactions. The resulting possibilities for neutrino-induced nucleosynthesis – or the ν -process – in massive stars are discussed. This includes two relatively recent extensions of ν -process calculations to heavier nuclei, one focused on understanding the origin of ^{138}La and ^{180}Ta and the second on the effects following r -process freezeout. From calculations of the neutrino post-processing of the r -process distribution, limits can be placed on the neutrino fluence after freezeout and thus on the dynamic timescale for the expansion.

1 Basic Supernova Neutrino Characteristics

A massive star, perhaps 15-25 solar masses, evolves through hydrostatic burning to an “onion-skin” structure, with a inert iron core produced from the explosive burning of Si. When that core reaches the Chandrasekar mass, the star begins to collapse. Gravitational work is done on the infalling matter, the temperature increases, and the increased density and elevated electron chemical potential begin to favor weak-interaction conversion of protons to neutrons, with the emission of ν_e s. Neutrino emission is the mechanism by which the star radiates energy and lepton number. Once the density exceeds $\sim 10^{12}$ g/cm³ in the infall of a Type II supernova, however, neutrinos become trapped within the star by neutral-current scattering,

$$\tau_{\nu}^{diffusion} \gtrsim \tau^{collapse} \quad (1)$$

That is, the time required for neutrinos to random walk out of the star exceeds $\tau^{collapse}$. Thus neither the remaining lepton number nor the gravitational energy released by further collapse can escape.

After core bounce a hot, puffy protoneutron star remains. Over times on the order of a few seconds, much longer than the 100s of milliseconds required for collapse, the star gradually cools by emission of neutrinos of all flavors. As the neutrinos diffuse outward, they tend to remain in flavor equilibrium through reactions such as

$$\nu_e + \bar{\nu}_e \leftrightarrow \nu_{\mu} + \bar{\nu}_{\mu} \quad (2)$$

producing a rough equipartition of energy/flavor. Near the trapping density of 10^{12} g/cm³ the neutrinos decouple, and this decoupling depends on flavor due to the different neutrino-matter cross sections,

$$\begin{aligned} \nu_x + e &\leftrightarrow \nu_x + e : \sigma_{\nu_{\mu}} / \sigma_{\nu_e} \sim 1/6 \\ \nu_e + n &\leftrightarrow p + e^+ \\ \bar{\nu}_e + p &\leftrightarrow n + e^+. \end{aligned} \quad (3)$$

One concludes that heavy-flavor neutrinos, because of their weaker cross sections for scattering off electrons (and the absence of charged-current reactions off nucleons), will decouple at higher densities, deeper within the protoneutron star, where the temperature is higher. In the case of electron neutrinos, the ν_e s are more tightly coupled to the matter than the $\bar{\nu}_e$ s, as the matter

is neutron rich. The result is the expectation of spectral differences among the flavors. If spectral peaks are used to define an effective Fermi-Dirac temperature, then supernova models [1] typically yield values such as

$$\begin{aligned} T_{\nu_\mu} &\sim T_{\nu_\tau} \sim T_{\bar{\nu}_\mu} \sim T_{\bar{\nu}_\tau} \sim 8MeV \\ T_{\nu_e} &\sim 3.5MeV \quad T_{\bar{\nu}_e} \sim 4.5MeV \end{aligned} \tag{4}$$

Some of the issues relevant to subsequent neutrino-induced nucleosynthesis include:

- The ν_e and $\bar{\nu}_e$ temperatures are important for the p/n chemistry of the “hot bubble” where the r-process is thought to occur. This is high-entropy material near the mass-cut that is blown off the protoneutron star by the neutrino wind.
- Matter-enhanced neutrino oscillations, in principle, could generate temperature inversions affecting p \leftrightarrow n charge-current balance, thus altering conditions in the “hot bubble” necessary for a successful *r*-process.
- If the “hot bubble” is the *r*-process site, then synthesized nuclei are exposed to an intense neutrino fluence that could alter the r-process distribution. The relevant parameter is the neutrino fluence after r-process freezeout.

2 New Neutrino Physics Discoveries and Potential Supernova Implications

Following the chlorine, GALLEX/SAGE, and Kamioka/Super-Kamiokande experiments, strong but circumstantial arguments led to the conclusion that the data indicated new physics. For example, it was observed that, even with arbitrary adjustments in the undistorted fluxes of pp, ${}^7\text{Be}$, and ${}^8\text{B}$ fluxes, the experimental results were poorly reproduced [2]. When neutrino oscillations were included, however, several good fits to the data were found. These included the small-mixing-angle (SMA) and large-mixing-angle (LMA) MSW solutions, the LOW solution, and even the possibility of “just-so” vacuum oscillations, where the oscillation length is comparable to the earth-sun separation. The ambiguities were convincingly removed by the charged- and neutral-current results of SNO, which demonstrated that about 2/3rds of the solar neutrino flux was carried by heavy-flavor neutrinos [3].

Similarly, anomalies in atmospheric neutrino measurements – a zenith-angle dependence in the ratio of electron-like to muon-like events – indicated

a distance-dependence in neutrino survival properties consistent with oscillations. The precise measurements of Super-Kamiokande provided convincing evidence for this conclusion, and thus for massive neutrinos [4].

A summary of recent discoveries in neutrino physics include:

- Oscillations in matter can be strongly enhanced.
- SNO identified a unique two-flavor solar neutrino solution corresponding to $\theta_{12} \sim \pi/6$ and $\delta m_{12}^2 \sim 7 \times 10^{-5} \text{ eV}^2$.
- The KamLAND reactor $\bar{\nu}_e$ disappearance experiment has confirmed the SNO conclusions and narrowed the uncertainty on δm_{12}^2 [5].
- The Super-Kamiokande atmospheric neutrino results show that those data require a distinct $\delta m_{23}^2 \sim (2 - 3) \times 10^{-3} \text{ eV}^2$ and a mixing angle $\theta_{23} \sim \pi/4$ that is maximal, to within errors.
- The KEK-to-Kamioka oscillation experiment K2K is consistent with the Super-Kamiokande atmospheric results, finding $\delta m_{23}^2 \sim (1.5 - 3.9) \times 10^{-3} \text{ eV}^2$ under the assumption of maximal mixing [6].
- Chooz and Palo Verde searches for reactor $\bar{\nu}_e$ disappearance over the δm_{23}^2 distance scale have provided null results, limiting θ_{13} [7].

These results have determined two mass splittings, δm_{12}^2 and the magnitude of $|\delta m_{23}^2|$. But as only mass differences are known, the overall scale is undetermined. Likewise, because the sign of δm_{23}^2 is so far unconstrained, two mass hierarchies are possible: the “ordinary” one where the nearly degenerate 1,2 mass eigenstates are light while eigenstate 3 is heavy, and the inverted case where the 1,2 mass eigenstates are heavy while eigenstate 3 is light. The relationship between the mass eigenstates (ν_1, ν_2, ν_3) and the flavor eigenstates (ν_e, ν_μ, ν_τ) is given by the mixing matrix, a product of the three rotations 1-2 (solar), 1-3, and 2-3 (atmospheric):

$$\begin{aligned} \begin{pmatrix} \nu_e \\ \nu_\mu \\ \nu_\tau \end{pmatrix} &= \begin{pmatrix} c_{12}c_{13} & s_{12}c_{13} & s_{13}e^{-i\delta} \\ -s_{12}c_{23} - c_{12}s_{23}s_{13}e^{i\delta} & c_{12}c_{23} - s_{12}s_{23}s_{13}e^{i\delta} & s_{23}c_{13} \\ s_{12}s_{23} - c_{12}c_{23}s_{13}e^{i\delta} & -c_{12}s_{23} - s_{12}c_{23}s_{13}e^{i\delta} & c_{23}c_{13} \end{pmatrix} \begin{pmatrix} \nu_1 \\ \nu_2 \\ \nu_3 \end{pmatrix} \\ &= \begin{pmatrix} 1 & & \\ & c_{23} & s_{23} \\ & -s_{23} & c_{23} \end{pmatrix} \begin{pmatrix} c_{13} & s_{13}e^{-i\delta} \\ & 1 \\ -s_{13}e^{i\delta} & c_{13} \end{pmatrix} \begin{pmatrix} c_{12} & s_{12} \\ -s_{12} & c_{12} \\ & & 1 \end{pmatrix} \begin{pmatrix} \nu_1 \\ e^{i\phi_1}\nu_2 \\ e^{i\phi_2}\nu_3 \end{pmatrix} \end{aligned} \quad (5)$$

Here $s_{12} = \sin \theta_{12}$, etc. We see, in addition to the unknown third mixing angle θ_{13} , this relationship depends on one Dirac CP-violating phase parameterized by δ and two Majorana CP-violating phases parameterized by ϕ_1 and ϕ_2 . The

former could be measured in long-baseline neutrino oscillation experiments (with the ease of this depending on the size of s_{13}), while the latter could influence rates for double beta decay.

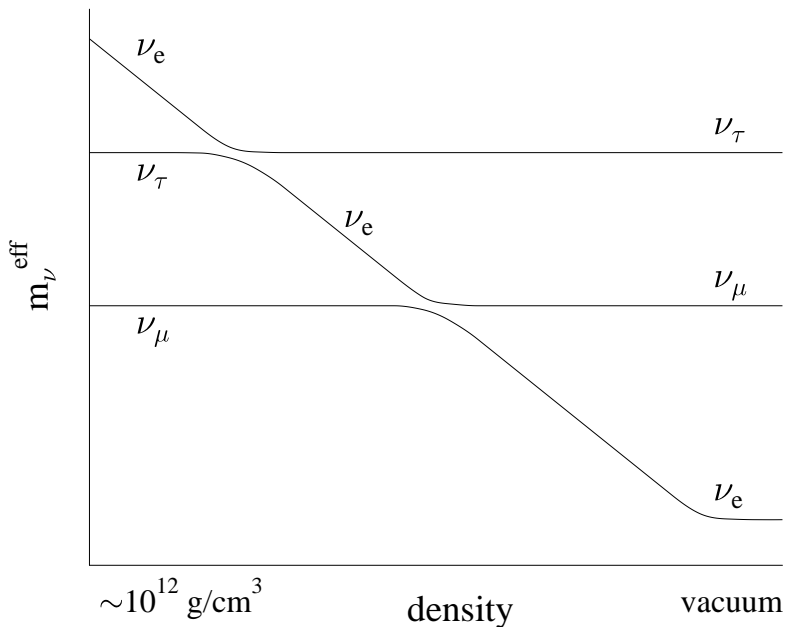


Figure 1: A three-level MSW level-crossing diagram showing the second crossing that should occur at densities characteristic of the base of the carbon zone in a Type II supernova progenitor star.

These new neutrino physics discoveries could have a number of implications for supernova physics:

- Because of solar neutrinos, we have been able to probe matter effects up to densities $\rho \sim 100 \text{ g/cm}^3$ characteristic of the solar core. As the density at the supernova neutrinosphere is $\rho \sim 10^{12} \text{ g/cm}^3$, supernova neutrinos propagate in an MSW potential that can be 10 orders of magnitude greater than any we have tested experimentally. In addition, the neutrinos propagate in a dense neutrino background, generating new MSW potential contributions due to $\nu-\nu$ scattering. Such effects, as well as the magnitude of the ordinary-matter MSW effects, may be unique to the supernova environment.
- We do not know θ_{13} , which is the crucial mixing angle for supernovae. This

angle governs the ν_e -heavy flavor level crossing encountered at depth in the star. This crossing occurs near the base of the carbon zone in the progenitor star, and remains adiabatic for $\sin^2 2\theta_{13} \gtrsim 10^{-4}$. For the ordinary hierarchy, the resulting $\nu_e \leftrightarrow \nu_{\mu,\tau}$ crossing would lead to a hotter ν_e spectrum. For an inverted hierarchy, the crossing would be $\bar{\nu}_e \leftrightarrow \bar{\nu}_{\mu,\tau}$.

- Presumably the position of this crossing will be influenced by the neutrino background contribution to the MSW potential. This nonlinear problem is rather complicated because the flavor content of the background evolves with time (being ν_e -dominated at early times).

3 Nuclear Structure Issues

Inelastic neutrino-nucleus interactions are important to a range of supernova problems, including neutrino nucleosynthesis, the detection of supernova neutrinos in terrestrial detectors, and neutrino-matter heating that could boost the explosion. The heavy-flavor neutrinos have an average energy $\langle E \rangle \sim 3.1T \sim 25$ MeV. However the most effective energy for generating nuclear transitions can be substantially higher because cross sections grow with energy and because nuclear thresholds are more easily overcome by neutrinos on the high-energy tail of the thermal distribution.

For the neutrino energy range of interest the allowed approximation, which includes only the Gamow-Teller $g_A \sigma(i) \tau_{\pm}(i)$ and Fermi $\tau_{\pm}(i)$ operators, is often not adequate. (These are given for charge-current reactions; the allowed operator for inelastic neutral current reactions is $g_A \sigma(i) \tau_3(i)$.) Important additional contributions come from operators that depend on the three-momentum transfer q , which can approach twice the neutrino energy, for back-angle scattering. Consequently qR , where R is the nuclear size, may not be small. Such first-forbidden contributions may be as important as the allowed contribution for supernova $\nu_{\mu}S$ and $\nu_{\tau}S$.

For all but the lightest nuclei, cross sections must be estimated from nuclear models, such as the shell model. Shell model wave functions are generated by diagonalizing an effective interaction in some finite Hilbert space of Slater determinants formed from shells $|n(ls)jm_j\rangle$. The space may be adequate for describing the low-momentum components of the true wave function, but not the high-momentum components induced by the rather singular short-range NN potential. The effective interaction, usually determined empirically, is a low-momentum interaction that corrects for the effects

of the excluded, high-momentum excitations. Similarly, effective operators should be used in evaluating matrix elements, such as those of the weak interaction operators under discussion here, and the shell model wave function should have a nontrivial normalization. In effective interaction theory, that normalization is the overlap of the model-space wave function with the true wave function.

Because effective interaction theory is difficult to execute properly – in some sense it is as difficult as solving the original problem in the full, infinite Hilbert space – nuclear modelers take short cuts. Often all effective operator corrections are ignored: bare operators are used. In other cases, phenomenological operator corrections can be deduced from systematic comparisons of shell-model predictions and experimental data.

The Gamow-Teller operator is an interesting case. Rather thorough comparisons of $2s1d$ and $2p1f$ shell-model predictions with measured allowed β -decay rates have yielded a simple, phenomenological effective operator: the axial coupling $g_A^{eff} \sim 1.0$ should be used rather than the bare value [8, 9]. This observation is the basis for many shell-model estimates of the Gamow-Teller response that governs allowed neutrino cross sections. Many of the shell-model techniques are quite powerful. Moments techniques based on the Lanczos algorithm [9] have been used to treat spaces of dimension $\sim 10^8$: important supernova neutrino cross sections for Fe and Ni isotopes have been derived in this way [10]. Another shell-model-based method uses Monte Carlo sampling [11].

There are reasons to have less confidence in corresponding estimates of first-forbidden effective operators. The first-forbidden operators include the vector operator $qr(i)$ and the axial-vector operators $[q \otimes r(i)]_{0,1,2}$. Electron scattering and photo-absorption provide tests of the vector operator, but direct probes of the axial responses are lacking. Unitarity is also an issue. Standard shell-model spaces satisfy the sum-rule constraints for the Gamow-Teller operator: the operator cannot generate transitions outside a full shell, for example. In contrast, for harmonic-oscillator Slater determinants, the first-forbidden operators generate transitions for which $\Delta N = \pm 1$, where N is the principal quantum number. Thus, underlying sum rules are violated as the operators always connect either initial or final configurations to states outside the shell-model space.

When the full momentum dependence of the weak interaction operators

is included, the resulting spin-spatial structure includes forms such as

$$j_l(qr(i))[Y_l(\Omega(i)) \otimes I_s]_{JM_J}$$

where j_l is a spherical Bessel function, Y_l a spherical harmonic, and I_s is a single-particle spin function. (More complicated forms involve vector spherical harmonics combined with spatial operators such as $\nabla(i)$.) The fact that q cannot then be factored from the operator then makes Lanczos moments techniques less useful: at every desired q the Lanczos procedure has to be repeated. (There are techniques under development [12] which exploit special properties of the harmonic oscillator to circumvent this problem.) Thus most calculations that treat the full momentum-dependence of the weak operators have used simple spaces, ones for which state-by-state summations of the weak transition strengths are practical. The approaches include truncated shell-model spaces, models based on the Random Phase Approximation (RPA), and even the highly schematic Goldhaber-Teller model.

Figure 2 compares continuum RPA results for charge-current reactions on ^{16}O with shell-model results of the sort described above [13]. The quantities plotted are cross sections averaged over a thermal neutrino spectrum. This is an interesting test case because ^{16}O , naively a closed-shell nucleus, has a smaller Gamow-Teller response than most mid-shell nuclei. Thus momentum-dependent contributions to the cross section should be more important than in many other cases. It is perhaps surprising, given the assumptions implicit in both the shell-model and CRPA calculations, that the results agree so well over the full range of interesting supernova neutrino temperatures. The only significant discrepancy, at very low temperatures, is due to the inclusion of contributions from ^{18}O in the shell model calculation used in Fig. 2. (The calculations were done for a natural oxygen target.) Due to the very low threshold for $^{18}\text{O} \rightarrow ^{18}\text{F}$, this minor isotope (0.2% relative to ^{16}O) dominates the $\text{O}(\nu_e, e)$ cross section at sufficiently low temperatures. The good agreement between the shell-model and CRPA calculations, of course, could mask problems associated with common assumptions, such as the absence of a reliable procedure for assessing effective operators beyond the allowed approximation.

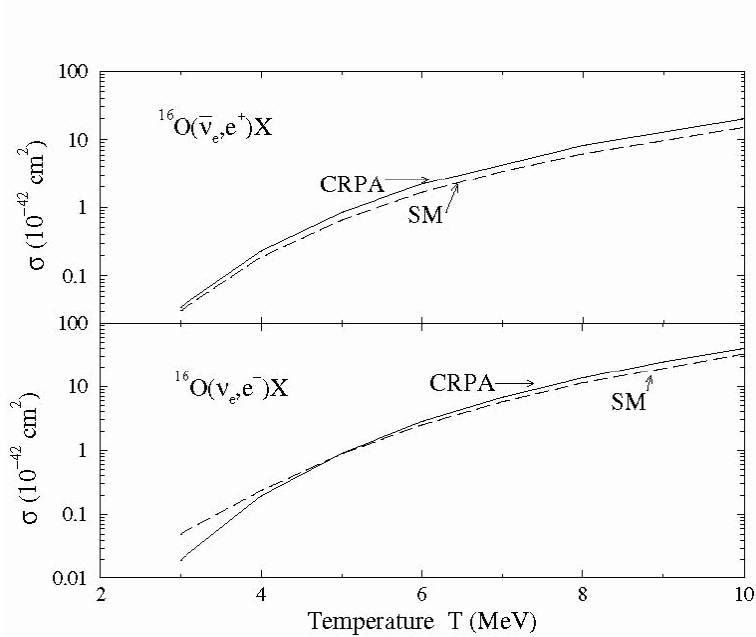


Figure 2: Comparison of CRPA (full lines) and shell-model (dash lines) cross section predictions, integrated over thermal neutrino spectra. The shell-model results include the contribution from ^{18}O , important at low temperatures in natural water for the (ν_e, e^-) reaction. From Kolbe, Langanke, Martinez-Pinedo, and Vogel [13].

4 The Neutrino Process

Several rare isotopes are thought to be created during a core-collapse supernova by neutrino reactions in the mantle of the star [14]. The most common mechanism is inelastic neutral-current neutrino scattering off a target nucleus like ^{20}Ne or ^{12}C , with significant energy transfer, e.g., giant resonance excitation. The nucleus, excited above the continuum, then decays by nucleon or α emission, leading to new nuclei. A nuclear network calculation is required to assess the survival of the neutrino-process products, such as ^{19}F in the Ne shell and ^{11}B in the C shell. The co-produced nucleons can capture back on the daughter nucleus, destroying the product of interest. Similarly, passage of the shock wave leads to heating that can destroy the product by (γ, α) and similar reactions. Frequently the majority of the instantaneous production is lost due to such explosive processing.

The enormous fluence of neutrinos can yield significant productions. Typically 1% of the nuclei in the deep mantle of the star – the C, Ne, and O shells – are transmuted by neutrinos. The most important products, like ^{19}F and ^{11}B , tend to be relatively rare odd-A isotopes neighboring very plentiful parent nuclei, such as ^{20}Ne and ^{12}C . (The parent isotopes are the hydrostatic burning products, typically.) The natural abundances of such odd-A isotopes could, in principle, be due to neutrino processing.

Such nucleosynthesis calculations must be embedded in a model of the supernova event. Important factors include:

- a neutrino flux that tends to diminish exponentially, with a typical time scale $\tau_\nu \sim 3$ sec;
- a pre-processing phase where nuclei in the mantle are exposed to the neutrino flux at some fixed radius r , prior to shock arrival;
- a post-processing phase after shock wave arrival, where the material exposed to the neutrino flux is heated by the shock wave (potentially destroying pre-processing productions), and then expands adiabatically off the star, with a temperature T that consequently declines exponentially;
- integration of these neutrino contributions into an explosive nucleosynthesis network; and
- integration over a galactic model, with some assumptions on the range of stellar masses that will undergo core collapse and mantle ejection.

Calculations of this nature were done by Woosley *et al.* [14]. Potentially significant neutrino-process productions include the nuclei ^{19}F , $^{10,11}\text{B}$, ^7Li , the gamma-ray sources ^{22}Na and ^{26}Al , ^{15}N , ^{31}P , ^{35}Cl , $^{39,40}\text{K}$, ^{51}V , and ^{45}Sc . Although the nuclear reaction network stopped at intermediate masses, the very rare isotopes ^{138}La and ^{180}Ta were also identified as likely ν -process candidates.

Recent work by Heger *et al.* [15] extends these calculations in important ways. First, the evolution of the progenitor star includes the effects of mass loss. Second, a reaction network is employed that includes all of the heavy elements through Bi, using updated reaction rates. Third, the nuclear evaporation process – emission of a proton, neutron, or α by the excited nucleus – is treated in a more sophisticated statistical model that takes into account known nuclear levels and their spins and parities. While the calculations lack a full set of neutrino cross sections, those cross sections important to known (*e.g.*, ^{19}F and ^{11}B) and suspected (*e.g.*, ^{138}La and ^{180}Ta) neutrino products were evaluated and incorporated into the network.

The results are shown in Fig. 3, with production factors normalized to

that of ^{16}O . Thus a production factor of one would mean that the ν -process would fully account for the observed abundance of that isotope. While ^{11}B might be slightly overproduced and ^{19}F slightly underproduced, given nuclear and astrophysics uncertainties, the ν -process yields of these isotopes and ^{138}La are compatible with this being their primary origin. The case of ^{138}La is particularly interesting, as the primary channel for the production is charged-current reaction $^{138}\text{Ba}(\nu, e)^{138}\text{La}$, where ^{138}Ba is enhanced in the progenitor star by the s -process. This production is the only known case where a charged-current channel dominates the production. Thus this yield is sensitive to the ν_e temperature – a potential indicator for oscillations if the transf

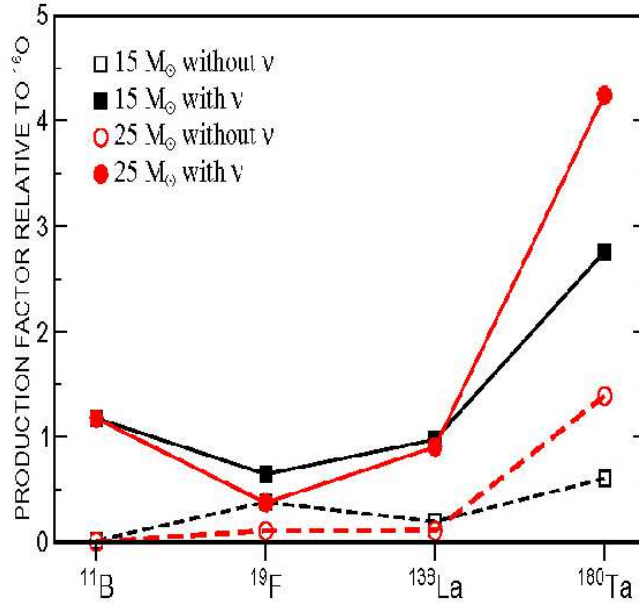


Figure 3: Neutrino-process production factors for ^{11}B , ^{19}F , ^{138}La , and ^{180}Ta , as calculated by Heger *et al.* [15]. The results are normalized to the production of ^{16}O in $15 M_{\odot}$ (squares) and $25 M_{\odot}$ (circles) progenitor stars. The open (filled) symbols represent stellar evolution studies in which neutrino reactions on nuclei were excluded (included).

While ^{180}Ta appears to be overproduced, the calculation does not distin-

guish production in the 9^- isomeric state from production in the 1^+ ground state. Only the isomeric fraction should be counted. An estimate of the ν -process fraction that ends up in the isomeric state, following a γ cascade, has not been made. However, initiating reactions such as $^{181}\text{Hf}(\nu_e, e^- n)$ involve low-spin parent isotopes, and the neutrino reaction transfers little angular momentum. Thus one would anticipate that the majority of the yield would cascade to the ground state. The reduction factor of 3-4 required to bring the ^{180}Ta production in line with the others of Fig. 3 is compatible with this.

There are other mechanisms for producing some of these ν -process products. One interesting one, for example, is cosmic-ray spallation reactions on CNO nuclei in the interstellar medium, which can produce $^{10,11}\text{B}$ and $^6,7\text{Li}$. Some such process is required to explain the origin of ^{10}B , for example. Cosmic-ray production, a secondary process, and the ν -process, a primary mechanism, might be distinguished by measurements that would separately determine the evolution of ^{10}B and ^{11}B . If the ν -process fraction of ^{11}B could be convincingly determined, this production would then become a more quantitative test of explosive conditions within the supernova carbon shell.

We note two recent observational results relevant to the ν -process. Prochaska, Howk, and Wolfe [16] recently observed over 25 elements in a galaxy at redshift $z = 2.626$, whose young age and high metallicity implies a nucleosynthetic pattern dominated by short-lived, massive stars. Their finding of a solar B/O ratio in an approximately 1/3-solar-metallicity gas argues for a primary (metal-independent) production mechanism for B such as the ν -process, rather than a secondary process. Similarly, new F abundance data of Cunha *et al.* show a low F/O ratio in two ω Centauri stars, which argues against AGB-star production of F (one competing suggestion), but would be consistent with the ν -process production [17].

5 Neutrino Process Effects in the r -process

Other speakers have discussed the r -process and the likelihood that the “hot bubble” – the high-entropy nucleon gas that is blown off the protoneutron star surface by the neutrino wind – is the primary site for the r -process. The nuclear physics of the r -process tells us that the synthesis occurs when the neutron-rich nucleon soup is in the temperature range of $(3 - 1) \times 10^9\text{K}$, which, in the hot bubble r -process, might correspond to a freeze-out radius

of (600-1000) km and a time ~ 10 seconds after core collapse. The neutrino fluence after freeze-out (when the temperature has dropped below 10^9 K and the r -process stops) is then $\sim (0.045 - 0.015) \times 10^{51}$ ergs/(100km) 2 . Thus, after completion of the r -process, the newly synthesized material experiences an intense flux of neutrinos. This suggests that ν -process postprocessing could affect the r -process distribution.

Comparing to our earlier discussion of carbon- and neon-zone synthesis by the ν -process, it is apparent that neutrino effects could be much larger in the hot bubble r -process: the synthesis occurs *much* closer to the star, at ~ 600 -1000 km. (The Ne-shell radius is $\sim 20,000$ km.) For this radius and a freezeout time of 10s, the “post-processing” neutrino fluence – the fluence that can alter the nuclear distribution after the r -process is completed – is about 100 times larger than that responsible for fluorine production in the Ne zone. As approximately 1/300 of the nuclei in the Ne zone interact with neutrinos, and noting that the relevant neutrino-nucleus cross sections scale roughly as A (a consequence of the sum rules that govern first-forbidden responses), one quickly sees that the probability of a heavy r -process nucleus interacting with the neutrino flux is approximately unity.

Because the hydrodynamic conditions of the r -process are highly uncertain, one way to attack this problem is to work backward [18]. We know the final r -process distribution (what nature gives us) and we can calculate neutrino-nucleus interactions relatively well. Thus by subtracting from the observed r -process distribution the neutrino post-processing effects, we can determine what the r -process distribution looked like at the point of freeze-out. In Fig. 4, the “real” r -process distribution - that produced at freeze-out - is given by the dashed lines, while the solid lines show the effects of the neutrino post-processing for a particular choice of fluence. The nuclear physics input into these calculations is precisely that previously described: GT and first-forbidden cross sections, with the responses centered at excitation energies consistent with those found in ordinary, stable nuclei, taking into account the observed dependence on $|N - Z|$.

One important aspect of Fig. 4 is that the mass shift is significant. This has to do with the fact that a 20 MeV excitation of a neutron-rich nucleus allows multiple neutrons (~ 5) to be emitted. (The binding energy of the last neutron in an r -process neutron-rich nuclei is about 2-3 MeV under typical r -process conditions.) The second thing to notice is that the relative contribution of the neutrino process is particularly important in the “valleys” beneath the mass peaks: the reason is that the parents on the mass peak are

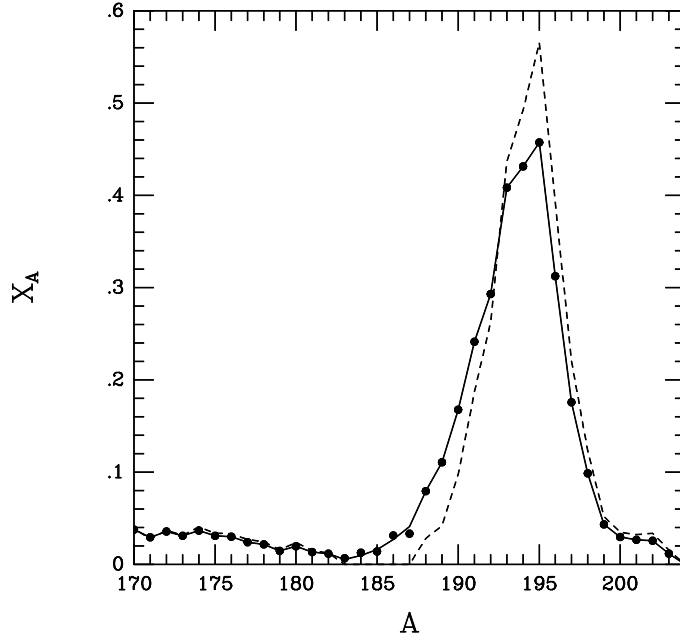


Figure 4: Comparison of the r -process distribution that would result from the freeze-out abundances near the $A \sim 195$ mass peak (dashed line) to that where the effects of neutrino post-processing have been included (solid line). The fluence has been fixed by assuming that the $A = 183$ - 187 abundances are entirely due to the ν -process.

abundant, and the valley daughters rare. In fact, it follows from this that the neutrino process effects can be dominant for precisely seven isotopes (Te, Re, etc.) lying in the valleys below the $A=130$ (not shown) and $A=195$ (Fig. 4) mass peaks. Furthermore if an appropriate neutrino fluence is picked, these isotope abundances are correctly produced (within abundance errors). The fluences are

$$\begin{aligned} N = 82 \text{ peak} & \quad 0.031 \cdot 10^{51} \text{ergs}/(100\text{km})^2/\text{flavor} \\ N = 126 \text{ peak} & \quad 0.015 \cdot 10^{51} \text{ergs}/(100\text{km})^2/\text{flavor}, \end{aligned}$$

values in fine agreement with those that would be found in a hot bubble r -process. So this is circumstantial but significant evidence that the material near the mass cut of a Type II supernova is the site of the r -process: there

is a neutrino fingerprint.

A more conservative interpretation of these results, however, places a bound on the r -process post-processing neutrino fluence by insisting that these isotopes not be overproduced. This bound will hold even if there are other mechanisms, such as neutron emission accompanying the β decay of r -process parent nuclei as they move to the valley of stability, that contribute to the abundances of these rare isotopes. This bound is then an interesting constraint on supernova dynamics: the neutrino fluence after freezeout depends on the flux at the time of freezeout and on the dynamic time scale (or the velocity of the material being expelled from the supernova). This constraint is plotted in Fig. 5 along with one imposed by the observed β -flow equilibrium of nuclei near the mass peak. (The β -flow equilibrium requires that the neutrino flux at freezeout not exceed the value where the neutrino reactions would compete with β decay. This would destroy the observed correlation between abundance and β decay lifetime.) Together these two constraints place upper bounds on the luminosity at freezeout (equivalently, a lower bound on the freezeout radius) and on the dynamic timescale.

6 Summary

This goal of this talk is to make some connections between supernova neutrino physics, the nuclear structure governing neutrino-nucleus interactions, and new neutrino properties. The main example used here, the neutrino process, connects observable abundances with supernova properties, such as the r -process freezeout radius and dynamic timescale. Thus by identifying ν -process products and by reducing the associated nuclear structure uncertainties that govern their abundances, one may be able to place significant constraints on the explosion mechanism.

The conditions for the r -process itself and for various ν -process productions are set by neutrino physics. For example, the p/n chemistry of the “hot bubble” is largely governed by charged-current $p \leftrightarrow n$ reactions, while the productions of ^{138}La and ^{19}F depend primarily on charged-current interactions on ^{138}Ba and on neutral-current reactions on ^{20}Ne , respectively. Thus in principle such productions could be influenced by oscillations that invert ν_e and heavy-flavor neutrino spectra (or, in the case of an inverted hierarchy, $\bar{\nu}_e$ and heavy-flavor antineutrino spectra). This is another important reason for exploring the nucleosynthetic “fingerprints” of supernova neutrinos. The

productions identified so far that would be influenced by neutrino oscillations, such as ^{138}La , are created at densities above those characterizing the naive 1-3 MSW matter crossing, at least in the pre-processing phase. However, we have noted that the location of MSW crossings could be perturbed by neutrino background effects. Furthermore, in the post-processing phase, crossings will arise in the rarified matter that expands off the star. This is a fascinating question for the r -process, and perhaps also for certain ν -process productions. These observations should motivated further studies of the potential effects of new neutrino physics on supernova nucleosynthesis.

This work was supported in part by the Office of Science, U.S. Department of Energy, under grants DE-FG02-00ER41132 and DE-FC02-01ER41187.

References

- [1] M. Liebendoerfer, M. Rampp, H.-Th. Janka, and A. Mezzacappa, astro-ph/0310662/ and to be published in *Ap. J.*; A. Burrows, astro-ph/0405427/.
- [2] K. M. Heeger and R. G. H. Robertson, *Phys. Rev. Lett.* **77**, 3720 (1996).
- [3] SNO Collaboration, *Phys. Rev. Lett.* **87**, 071301 (2001); **89**, 011301 (2002); **92**, 181301 (2004).
- [4] Super-Kamiokande Collaboration, *Phys. Rev. Lett.* **81**, 1562 (1998); **82**, 2644 (1999); **85**, 3999 (2000).
- [5] KamLAND Collaboration, *Phys. Rev. Lett.* **90**, 021802 (2003); **92**, 071301 (2004).
- [6] K2K Collaboration, *Phys. Rev. Lett.* **90**, 041801 (2003).
- [7] M. Apollonio *et al.*, *Phys. Lett. B* **420**, 397 (1998); F. Boehm *et al.*, *Phys. Rev. D* **64**, 112001 (2001).
- [8] B. A. Brown and B. H. Wildenthal, *At. Data Nucl. Data Tables* **33**, 347 (1985).
- [9] G. Martinez-Pinedo, A. Poves, E. Caurier, and A. P. Zucker, *Phys. Rev. C* **53**, 2602 (1996).

- [10] E. Caurier, K. Langanke, G. Martinez-Pinedo, and F. Nowacki, *Nucl. Phys. A* **653**, 439 (1999).
- [11] S. E. Koonin, D. J. Dean, and K. Langanke, *Phys. Repts.* **278**, 1 (1997); T. Otsuka, M. Honma, and T. Mizusaki, *Phys. Rev. Lett.* **81**, 1588 (1998).
- [12] W. C. Haxton, K. Nollett, and K. Zurek, in preparation.
- [13] E. Kolbe, K. Langanke, G. Martinez-Pinedo, and P. Vogel, *J. Phys. G* **29**, 2569 (2003).
- [14] S. E. Woosley and W. C. Haxton, *Nature* **554**, 45 (1988); S. E. Woosley, D. H. Hartmann, R. D. Hoffman, and W. C. Haxton, *Astroph. J.* **356**, 272 (1990); G. V. Domogatskii and D. K. Nadyozhin, *Sov. Astro.* **22**, 297 (1978).
- [15] A. Heger *et al.*, astro-ph/0307546/.
- [16] J. X. Prochaska, J. C. Howk, and A.M. Wolfe, *Nature* **423**, 57 (2003).
- [17] K. Cunha, V. V. Smith, D. L. Lambert, and K. H. Hinkle, *Astron. J.* **126**, 1305 (2003).
- [18] Y.-Z. Qian, W. C. Haxton, K. Langanke, and P. Vogel, *Phys. Rev. C* **55**, 1532 (1997); W. C. Haxton, K. Langanke, Y.-Z. Qian, and P. Vogel, *Phys. Rev. Lett.* **78**, 2694 (1997).

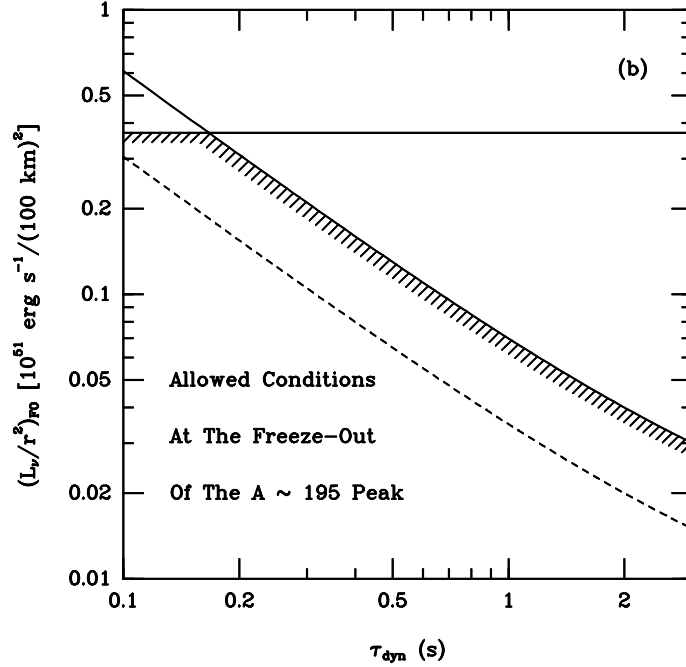


Figure 5: Constraints imposed on the neutrino flux parameter L_ν/r^2 at freezeout, where L_ν is the luminosity and r the freezeout radius, and on the dynamic timescale τ_{dyn} governing the expansion. The horizontal solid line results from the condition of β -flow equilibrium for the $A=195$ peak. The diagonal solid line is the requirement that ν -process post-processing of the r -process peak not overproduce nuclei in the mass region $A=183-187$. The calculation assumes a neutrino flux that evolves exponentially with $\tau_\nu = 3\text{s}$. Parameters lying on the dashed line corresponds to the fluence determined by attributing the full abundances of $A=183-187$ nuclei to the neutrino process.